ATMOSPHERIC ENVIRONMENT: X 13 (2022) 100154

Contents lists available at ScienceDirect

Atmospheric Environment: X

journal homepage: www.journals.elsevier.com/atmospheric-environment-x

Seasonal patterns in rice and wheat residue burning and surface $PM_{2.5}$ concentration in northern India

Carlo Montes [a,*], Tek Sapkota [a], Balwinder Singh [b]

[a] International Maize and Wheat Improvement Center (CIMMYT), Texcoco, Mexico
[b] International Maize and Wheat Improvement Center (CIMMYT), New Delhi, India

ARTICLE INFO

Keywords:
Air quality
Biomass burning
Emission inventory
Active fires
South asia

ABSTRACT

Rice-Wheat production system of the Indo-Gangetic Plain (IGP) in northern India generates large amounts of crop residues annually, substantial amount of which is burned *in-situ*. Due to this, people in this region and nearby cities are exposed to extremely high concentrations of atmospheric pollutants, especially in late autumn to winter. Multiple factors affect air quality, the main ones being pollutant emissions and meteorology. We generated a high-resolution ($0.05^\circ \times 0.05^\circ$) multi-year (2012–2020) fine particular matter ($PM_{2.5}$) dataset of pollutant emissions from wheat and rice residue burning for the IGP by combining production data and satellite active fires from the Visible Infrared Imaging Radiometer Suite (VIIRS) 375-m product. We used surface $PM_{2.5}$ concentrations and meteorological data from Modern-Era Retrospective Analysis for Research and Applications version 2 (MERRA-2) atmospheric reanalysis to characterize the seasonal $PM_{2.5}$ concentrations and their relationships with anomalies in meteorological conditions. Results showed a much higher number of fires during from rice, with an interannual average of 79,385 total fires versus 33,096 from wheat. Emissions are higher during the rice harvest period: 406 Gg/year versus 245 Gg/year, respectively for rice and wheat. Emissions and $PM_{2.5}$ concentrations from rice harvest are higher than those of wheat as a consequence of a higher number of fire spots, emissions, and atmospheric conditions that prevent their dispersion. $PM_{2.5}$ concentrations are in addition strongly related to the amount of biomass burned and the number of fires and their intensity. In terms of meteorological anomalies, the planetary boundary layer height, wind speed and the surface thermal inversion strength have a stronger association with $PM_{2.5}$ concentration during the rice residue burning period. Conversely, $PM_{2.5}$ concentration and emissions anomalies during the wheat harvest shows a stronger correlation with factors associated with the amount of residues burned in the field.

1. Introduction

The Indo-Gangetic Plain (IGP) in northern India, including capital of India, New Delhi city, is characterized by a high demographic and economic growth that has made this region a global hotspot of high pressure on natural resources and their deterioration. The latter includes the high exposure of population to declining air quality in a region that ranks among the ones with the highest air pollution levels in the world (IQAir, 2019). Every year, air pollution is responsible for acute health problems on population, especially during the cold and dry season, when reduced dispersion conditions associated with meteorology lead to recurrent episodes of extremely high concentrations of $PM_{2.5}$, the particulate matter with aerodynamic diameter lower than 2.5 μm (Gupta et al., 2016). At the same time, dominant rice-wheat rotations in the states of Punjab and Haryana, the so-called Indian "breadbasket", are the producing areas of two-thirds of food grains in India (Sekar and Pal, 2012).

Multiple natural and anthropogenic sources of pollutant emission are responsible for the current state of air quality in northern India, namely the burning of fossil fuels by industries and vehicles, forest and grassland fires, and the open field burning of crop residues. According to recent studies, the burning wheat and rice straw, the dominant cropping system, has become a major concern as it represents an increasing contribution to regional air pollution (Jethva et al., 2018; Liu et al., 2018a). Burning of rice and wheat residues is associated with a dramatic increase in pollutant emissions over the IGP (Sarkar et al., 2013; Kaskaoutis et al., 2014), generating air quality problems not only in the burning sites but also to distant cities when surface circulation favors the aerosol

* Corresponding author.
E-mail address: c.montes@cgiar.org (C. Montes).

https://doi.org/10.1016/j.aeaoa.2022.100154
Received 1 August 2021; Received in revised form 20 January 2022; Accepted 23 January 2022
Available online 29 January 2022

transport (Schnell et al., 2018). Of particular interest is the post-monsoon residue burning after *kharif* season crops are harvested, typically in October through December, given the coincidence between seasonal rainfall cessation and the reduction in the atmospheric dispersion capacity associated with lower air temperatures, shallow boundary layer and inversion layers, and lower pressure gradients, enhancing atmospheric pollution and air quality degradation (Schnell et al., 2018).

India has experienced a strong agricultural intensification to the increasing food demand, leading to higher crop productivity and consequently to higher residue generation on the fields (Jethva et al., 2019). Historically, these residues were manually removed from the field during harvesting by farmers (Kumar et al., 2015). With the advent of machine harvesting technologies, a significant amount of residues are currently left in the field. Although wheat residues are often taken off the field for animal feed, rice residues are considered waste and are burnt *in situ*. Burning is the preferred practices not only because of low management cost but also due to the short time window between rice harvest and wheat sowing (Kumar et al., 2015). The above suggests that the crop residue burning will increase unless residue management options are adopted by farmers (Ravindra et al., 2019). In this regard, recent studies by Balwinder Singh et al. (2019) and Sembhi et al. (2020) discussed about the implications of recent groundwater conservation policies on air quality over the IGP, highlighting the negative impact of delayed rice sowing and harvest dates on air quality after the increase in fire intensity later during the cold season.

Multiple studies have addressed the various aspects of crop residue burning and air pollution in northern India (e.g. Dey et al., 2012; Beig et al., 2020; Singh et al., 2020). Most of these have focused on the states of Punjab and Haryana and on the analysis of specific growing seasons, typically one or two years (Sahu et al., 2021). For instance, the significant local increase in atmospheric aerosols during the cold/dry season was characterized in Punjab and New Delhi by Mittal et al. (2009) and Pant et al. (2015), respectively, using a set of ground-level observations. Other studies have quantified regional $PM_{2.5}$ emissions from crop residue burning using non-spatially explicit approaches based on crop production statistics (Gadde et al., 2009; Ravindra et al., 2019), but they have not considered the influence of environmental factors drivers. However, patterns in crop biomass burning are highly variable given the high heterogeneity in crop management practices and size of agricultural exploitations, which makes it necessary to consider spatial aspects. In this sense, last generation satellite-based fire activity products are a widely-used source of information for regional biomass burning assessments and for the development of observational products. Dey et al. (2012) used satellite data from the Multiangle Imaging Spectro Radiometer (MISR) to identify and quantify hotpots of Indian population exposure to high air pollution levels. Also, active fire products from the Moderate Resolution Imaging Spectroradiometer (MODIS) and the Visible Infrared Imaging Radiometer Suite (VIIRS) sensors have been used to estimate emissions from crop residue burning over the IGP. For instance, Liu et al. (2018a) and Bray et al. (2019) used MODIS and ground-truth data to describe the role of particulate matter emissions from crop residue burning in northwest Indian cities and impacts on air pollution. Similarly, VIIRS data were used by Singh et al. (2020) to generate a gridded inventory of pollutants from crop residue burning in the state of Punjab. However, those studies focused only on the western states, not covering the whole transect of the IGP. Likewise, other variables such as Atmospheric Optical Depth (AOD) has been used to assess regional variability in air pollution in India (e.g. Kaskaoutis et al., 2014). Other studies combined satellite and ground information and atmospheric chemistry-transport models for the study of source contributions, time trajectories, and regional dispersion of pollutants (e.g. Liu et al., 2018a; Nair et al., 2020; Ojha et al., 2020).

This study focuses on the regional assessment of wheat and rice residue burning and associated emissions in the transect of the IGP (the states of Punjab, Haryana and Uttar Pradesh in India), using multiple data sources including VIIRS, crop statistics, and atmospheric global reanalysis, during both the wheat (pre-monsoon) and rice (post-monsoon) harvest periods when higher negative environmental impacts are expected. Specifically, (1) we implement a methodology for the spatial and multi-year characterization of seasonal patterns in $PM_{2.5}$ emissions from wheat and rice stubble burning and surface $PM_{2.5}$ concentrations, and (2) we assess the relationship between seasonal anomalies in $PM_{2.5}$ emissions and meteorological drivers of $PM_{2.5}$ concentrations in terms of planetary boundary layer height, wind speed and surface thermal inversion strength. This information will contribute to a better understanding of the spatial and temporal dynamics of air pollution and associated factors at time scales (seasonal) that has been little explored in the field of air pollution, and for which new investigations and products for monitoring and forecasting could be developed.

2. Materials and methods

2.1. Study area

The study area corresponds to the states of Punjab, Haryana and Uttar Pradesh in northern India (Fig. 1). This region, which covers a major part of the IGP, has the highest population density in India living both in a series of megacities and rural areas. The vast alluvial plains are mainly occupied by croplands, and rice-wheat rotation is the most typical cropping system. Crop residue burning is a widely-used practice, with significant impacts on people's health given the high population density. Additionally, the presence of high-elevation mountains to the North is a natural factor enhancing air pollution as a consequence of the channeling effect on surface circulation, which favors the transport of pollutants across the IGP (Schnell et al., 2018).

2.2. Datasets

2.2.1. Crop production data

Rice and wheat crop production data were obtained from the Indian

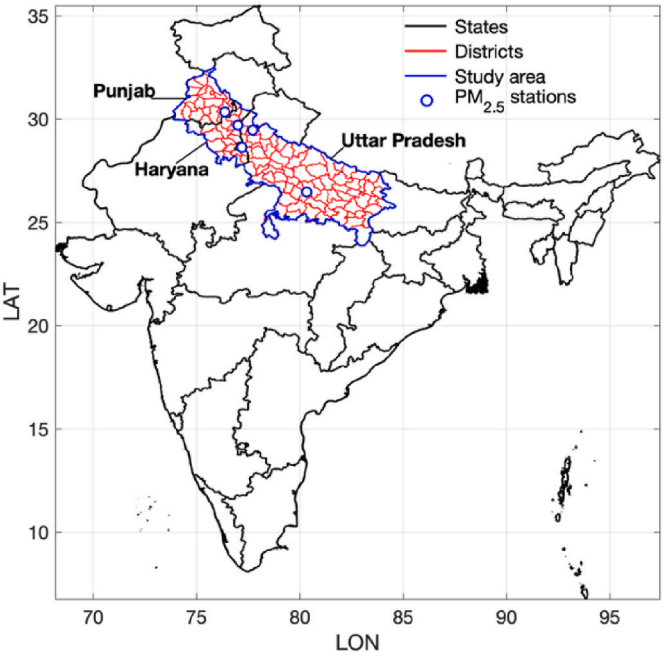

Fig. 1. Map of India showing the study area made up of the states of Punjab, Haryana and Uttar Pradesh. Red polygons correspond to districts (118 in total), the basic unit of crop production used in this study. Circles show the location of $PM_{2.5}$ stations. (For interpretation of the references to color in this figure legend, the reader is referred to the Web version of this article.)

Crop Production Statistics Information System (http://aps.dac.gov.in/APY/Index.htm). This dataset consists of district-level (Fig. 1) annual information statistics about cultivated species, varieties, annual production, surface and yields. In this study, total annual production data were extracted for the 118 districts that make up the states of Punjab, Haryana and Uttar Pradesh, for the years 2012 through 2020.

2.2.2. VIIRS fire spots and Fire Radiative Power

Fire counts data were collected from the Visible Infrared Imaging Radiometer Suite (VIIRS) sensor, which was launched in October 2011 onboard the NASA/NOAA Suomi-National Polar-orbiting (Suomi NPP) satellite. This product provides the geographical coordinates, time of the day, detection confidence (low, nominal, high), brightness temperature, Fire Radiative Power (FRP), and satellite view and solar zenith angles (Schroeder and Csiszar, 2014). VIIRS is a multi-spectral sensor (3040 km swath), providing global 375-m and 750-m spatial resolution radiances every 12 h (1:30 h and 13:30 h, local time), depending on the latitude, for fire-sensitive channels. We use active fire product data (VNP14IMG; 375-m resolution for the I-bands, and 750-m resolution for the M-bands), which are generated from land surface brightness temperatures above the 367 K saturation value measured by the 375-m radiances. FRP are derived using 375-m fire pixels and adjacent 750-m radiances from the M-band. VIIRS active fire data have been widely used for the study of fires of different origin, and has been reported as better suited for the study of small-scale fires than MODIS given its higher resolution and sensing geometry (Li et al., 2020).

2.2.3. MODIS land cover

Although the cropland land use is dominant over the study area, fire counts captured by VIIRS may fall within non-agricultural areas (e.g. cities, forests), so that these fire locations should be removed from the final dataset. For this, the yearly 500 m × 500 m spatial resolution MODIS MCD12Q1 V06 land cover product (Friedl et al., 2010) was used to remove all fire count outside the land use of interest. From the 17 MODIS land classes, only VIIRS active fires detections within land cover classes defined as "Cropland" and "Cropland Natural Vegetation Mosaics" were retained and used for further analyzes.

2.2.4. MERRA-2 atmospheric reanalysis

Data from the Modern-Era Retrospective Analysis for Research and Applications version 2 (MERRA-2) reanalysis, the update of the MERRA-1 version that was active until 2016, developed by the NASA Global Modeling and Assimilation Office (GMAO) were used for regional characterization of $PM_{2.5}$ concentrations and meteorology. MERRA-2 is a global reanalysis providing atmospheric and land surface variables, along with atmospheric composition, for climate and hydrological applications spanning the satellite era from 1979 to present at 0.5° × 0.625° spatial resolution for 72 vertical levels and for different time resolutions (from hourly to monthly) (Rienecker et al., 2011). MERRA-2 takes advantage of the Goddard Earth Observing System Data Assimilation System Version 5 (GEOS-5) Earth System model and earth observing satellites for atmospheric, oceanic, biogeochemical and land surface processes, and the Goddard Chemistry, Aerosol, Radiation, and Transport model (GOCART; Chin et al., 2002) to retrieve atmospheric composition and processes, including the assimilation of Terra and Aqua MODIS AOD.

We used near-surface hourly mass aerosol concentration from the MERRA-2 single-layer product, consisting of five aerosols species concentration within the lowest layer of the model: dust, sea salt, black and organic carbon, and sulfate. These five aerosol types were aggregated to estimate $PM_{2.5}$ mass concentration (kg m^{-3}) using the equation proposed by Buchard et al. (2016):

$$PM_{2.5} = [DS_{2.5}] + [SS_{2.5}] + [BC] + [OC] \times 1.4 + [SO_4] \times 1.375 \quad (1)$$

where $[DS_{2.5}]$, $[SS_{2.5}]$, $[BC]$, $[OC]$, and $[SO_4]$ are the mass concentration (mass/volume) of dust, salt, black carbon, organic carbon, and sulfate, respectively. The 2.5 in *DS* and *SS* denotes for particulate matter of size less than or equal to 2.5 μm. Factors 1.375 and 1.4 account for differences in the chemical representation of the sulfate ion and the contribution from other organic matter elements in GEOS-5 and MERRA-2, respectively (Buchard et al., 2016).

Along with the above presented $PM_{2.5}$ components, we used MERRA-2 hourly meteorological data of selected variables influencing $PM_{2.5}$ concentrations including planetary boundary layer height (m), 10-m zonal and meridional wind components (m s^{-1}), from which wind speed was calculated, surface layer height (m), 2-m air temperature, and 2-m air dewpoint temperature. Also, MERRA-2 2-m and 850-hPa air temperature data were used to calculate the temperature inversion strength as the difference between upper (850-hPa) and surface (2-m) air temperature (Gutiérrez et al., 2013; Schnell et al. 2018). Dewpoint and air temperature were used to calculate relative humidity from the widely-used equation involving actual and saturated vapor pressure (Allen et al., 1998). Although precipitation is an important factor modifying concentrations of atmospheric pollutants, we have focused on main variables influencing the dispersion of aerosols during the dry season, since both wheat and rice harvest periods occur after the monsoon withdrawal.

2.2.5. In-situ PM2.5 measurements

Ground-based hourly observations of surface $PM_{2.5}$ concentrations were obtained from the Central Pollution Control Board (CPCB) of India for a set of five stations located over the IGP, which are displayed in Fig. 1. CPCB data have been previously used for ambient $PM_{2.5}$ characterization (Chowdhury et al., 2019) and regional validation of gridded products such as MERRA-2 (Navinya et al., 2020). Data during the two periods of interest were used (April–May and October–November), and for 2018 and 2019, the available CPCB years. Since a detailed comparison and validation of MERRA-2 over the study area is out of the scope of this work, CPCB data were used to perform a general characterization of the differences between ground-truth observations and MERRA-2.

2.3. Estimating pollutant emissions from crop residue burning

The procedure for estimating $PM_{2.5}$ emissions from crop residue burning consists of two steps. Firstly, district-wise annual biomass burned and emissions using crop production statistics as the main data source are calculated. Secondly, satellite active fires are used to temporally allocate annual emissions at a daily time step and to aggregate district-wise values to a regular (0.05° × 0.05°) grid, as detailed below.

2.3.1. District-level $PM_{2.5}$ emissions

$PM_{2.5}$ emissions from crop residue burning were estimated at district level following the approach proposed by Streets et al. (2005) and adopted by multiple authors, namely in Azhar et al. (2019) and Zhang et al. (2019). This method, primarily based on total crop production and a set of parameters allowing the conversion from biomass to emissions, expresses initially the total mass emissions as the product between crop biomass burned in the field (*M*; kg) and a pollutant species-specific emission factor (*EF*; the mass of $PM_{2.5}$ emitted per unit of total mass consumed; g/kg) for each crop as:

$$E = M \times EF \times 10^{-9} \quad (2)$$

where *E* corresponds to the total $PM_{2.5}$ emissions from crop residue burning in mass units (Gg in this case). The district-level total biomass burned per season is estimated for wheat and rice based on crop production as:

$$M = P \times N \times D \times B \times F \quad (3)$$

where *P* is the district total crop production, *N* the residue to product

ratio, D the dry matter content fraction, B the fraction of residues that are burned in the field, and F the crop-specific combustion efficiency. Parameters used in Eqs. (2) and (3) are presented in Table 1, which were taken from previous works on biomass burning estimations in India. These parameters were generated from multiple local and regional field measurements following recommendations from the International Panel on Climate Change (Sahai et al., 2007; Streets et al., 2005; Gadde et al., 2009; Jain et al., 2014; Ravindra et al., 2019; Vadrevu and Lasko, 2018). Likewise, EF in Eq. (2) for $PM_{2.5}$ emissions from wheat and rice were adopted from studies over the same region and from recently-updated compilations for agricultural residues (Hays et al., 2005; Andreae, 2019; Ravindra et al., 2019).

2.3.2. Spatial and temporal allocation of $PM_{2.5}$ emissions

Total annual (2012–2020) $PM_{2.5}$ emissions were temporally and spatially allocated to a regular $0.05^\circ \times 0.05^\circ$ spatial resolution grid, using space-explicit VIIRS active fires. Firstly, a binary mask was generated from MCD12Q1 product in order to remove VIIRS points falling in a non-crop land cover. Secondly, $PM_{2.5}$ emissions obtained from 2.3.1 were aggregated using daily VIIRS fire counts and the following approach:

$$E_i = \frac{FC_i}{FC_d} \times E_d \quad (4)$$

where E_i represents the emissions of the i-th VIIRS detected fire, FC_i the fire count of the i-th grid, FC_d the total number of fire counts for the d district, and E_d the total emissions from district d (Eq. (2)).

The periods of stubble burning depends on the timing of harvesting. In the Indian states considered in this study, the wheat harvest typically begins in April and ends in May, while rice harvest peaks from November to December (Sahu et al., 2015; Liu et al., 2020). After the harvest, farmers generally burn the stubble left the fields to prepare the land for the next crop. Consequently, considering rice-wheat rotations as the main crop system, the study period for the temporal allocation of $PM_{2.5}$ emissions from these two dominant crops were set to October–November and April–May for rice and wheat, respectively.

2.4. Analysis

The first section of the results presents an overview of the main features of the regional, seasonal and interannual variability of the occurrence of fires associated with the burning of rice and wheat biomass, captured by the VIIRS product, and the $PM_{2.5}$ emissions calculated using the methodology explained above. Secondly, regional MERRA-2 $PM_{2.5}$ concentrations are described and compared against ground truth-based observations, summarized for the wheat and rice biomass burning periods. A third section corresponds to the analysis of the relationship between seasonal anomalies in MERRA-2 $PM_{2.5}$ concentrations, fire seasonal metrics, and the selected meteorological variables. The latter includes a Principal Component Analysis (PCA) applied to the centered and variance-scaled regionally integrated anomalies of $PM_{2.5}$ and meteorological variables in order to further explore how these variables are related on a seasonal basis.

Table 1
Parameters used in Eq. (2) to estimate $PM_{2.5}$ emissions.

Crop	Residue to product ratio (N^a)	Dry matter fraction (D^a)	Fraction of residue burned (B^a)	Combustion efficiency (F^a)	Emission factors (EF^b)
Wheat	1.75	0.88	0.8	0.86	7.6
Rice	1.5	0.86	0.25	0.89	12.95

[an] Expressed in fraction units.
[b] Expressed in g/kg of dry matter.

3. Results and discussion

3.1. Regional features of fire spots and $PM_{2.5}$ emissions from crop residue burning

Time series of regional average fire counts detected by 375-m VIIRS are presented in Fig. 2, along with the corresponding values of FRP, which is the measured rate of radiant energy released from a detected fire. Fig. 2a and b shows two peaks in fire occurrence and FRP that concentrate during April–May and October–November, which are mainly associated with the burning of wheat and rice residues, respectively. A very weak occurrence of fires during the cold season (December to March) is observed, which fluctuate at low values until the wheat harvest period in April–May. In summer, the monsoon rains prevent the emergence of both anthropogenic and natural fires. It is also observed that the number of fires and consequently FRP during the rice harvest time doubles those detected during the wheat harvest period and the annual course of sum of FRP indicates a similar amount of energy released per detected fire (Fig. 2c). Furthermore, the probability density function of normalized FRP (Fig. S1) shows a higher occurrence of fires in the average intensity range (FRP ~5 MW km^{-2}) but more fires of high energy released are observed in wheat (mean FRP 6.7 MW km^2) than rice (mean FRP 5.8 MW km^2). The above differences may be explained by the set of factors that explain emissions, including the amount of biomass burned, emission factors, combustion efficiency, straw composition, and also the timing of fires, since straw with higher moisture content exhibits more incomplete combustion (Roberts et al., 2009).

Maps of annual spatial distribution of density of number of fires (2012–2020) for wheat and rice are presented in Fig. 3, where values represent the number of fires within each $0.05^\circ \times 0.05^\circ$ grid point. A high density of crop residue fires is observed in the states of Punjab and Haryana, two of the most agriculturally intensive states in India. This pattern is consistent with previous inventories using high resolution VIIRS active fires for different spatial and temporal domains (Singh et al., 2020). Also, it is observed that the east area of Uttar Pradesh presents a relatively high concentration of fires and emissions associated with the burning of wheat stubble. For the case of rice residue burning (Fig. 3b), in addition to the higher regional number of fires counts, a higher concentration is observed in Punjab and Haryana, while these are notably lower in Uttar Pradesh in relation to wheat. The latter is likely due to the fact that rice farmers in Uttar Pradesh take rice residues off the field for livestock feeding instead of burning (Bhattacharyya et al., 2021). Further, wheat sowing in Uttar Pradesh is done late in autumn than in Haryana and Punjab thus giving relatively wider window for residue management. On the other hand, a similar annual spatial distribution of number of fire spots during the 9-year period is observed in Fig. 3, although some important variations such as the reduction in the maximum and average number of fires of rice residue burning between 2016 and 2017. It is also observed that the spatial distribution of number of fires is organized following the seasonal pattern of rice and winter wheat cultivation, which does not vary significantly from one year to another. The average interannual number of fires are 33,096 (standard deviation = 7561) and 79,385 (standard deviation = 14,318) for wheat and rice fires, respectively, values that are within the observed range of previous works over the region (Vadrevu and Lasko, 2018).

Maps of regional $PM_{2.5}$ emissions from wheat and rice residue burning are displayed in Fig. 4, where values correspond to the sum of emissions from each fire captured by VIIRS within each grid cell. Along with the higher emissions associated with a higher number of fires over Punjab and Haryana, and eastern Uttar Pradesh for the case of wheat residues, Fig. 4 shows a greater amount of emissions from rice stubble burning compared to wheat that is proportional to the difference in number of fires (Fig. 3). Despite the considerable amount of residues generated by the wheat harvest, a significant amount of them are removed from the fields for animal feeding, unlike rice straw, of which a

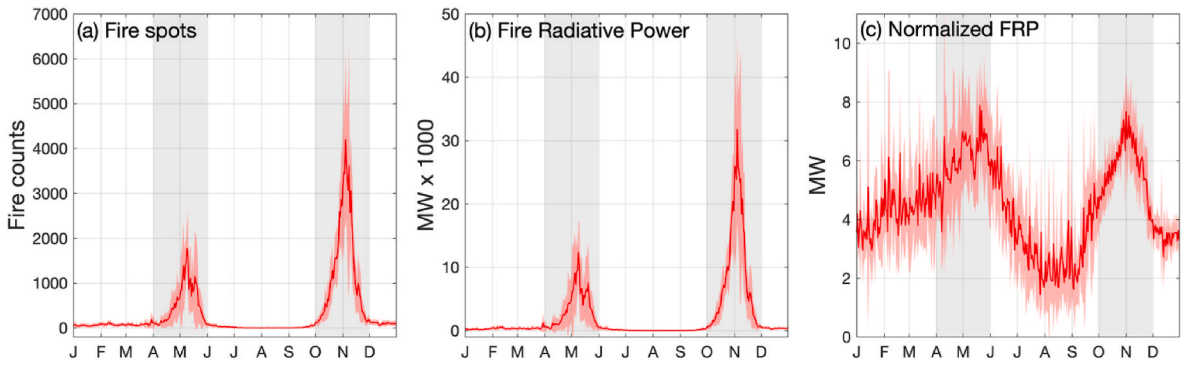

Fig. 2. (a) Interannual (2012–2020) regional average (solid line) and standard deviation (red area) of (a) daily number of fire sports, (b) daily spatially accumulated FRP and (c) FRP normalized by the number of fire spots. Gray area represents the temporal window of wheat (April–May) and rice (October–November) harvest and residue burning. Abscissa labels denote the beginning of each month. (For interpretation of the references to color in this figure legend, the reader is referred to the Web version of this article.)

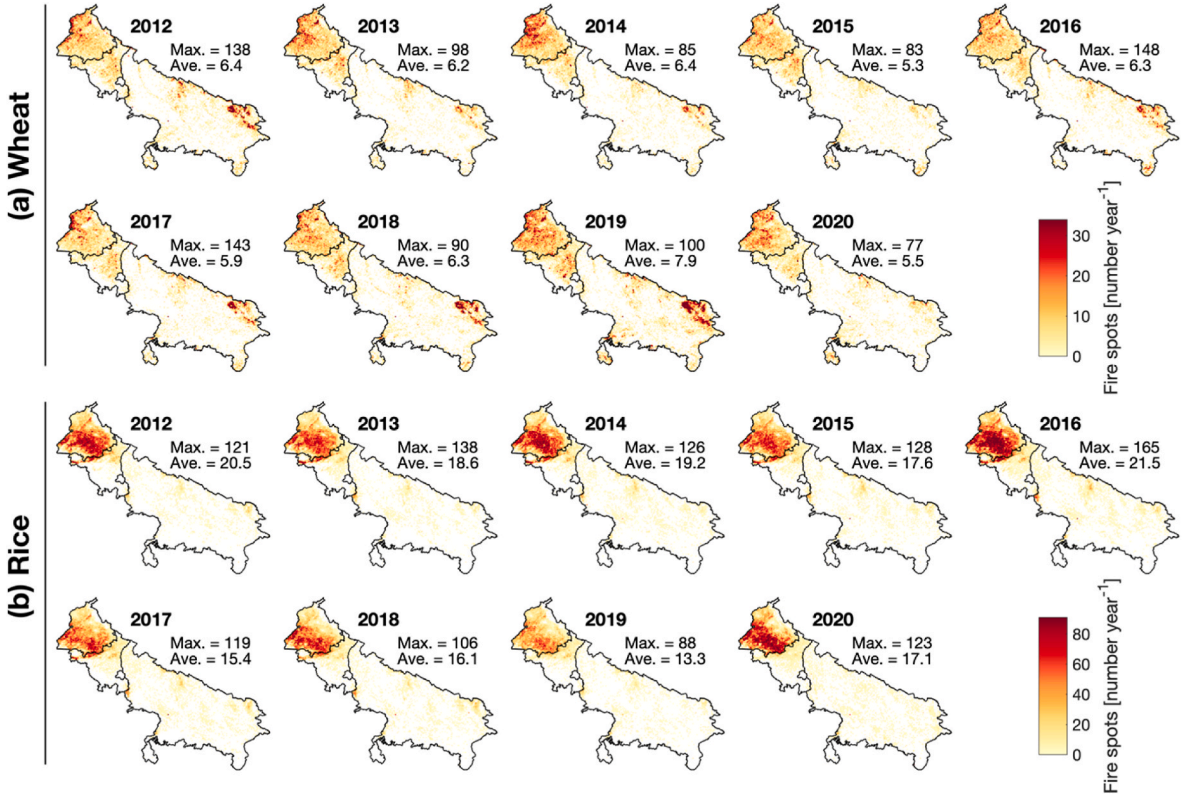

Fig. 3. Maps of fire spots density (per grid; 2012–2020) associated with wheat and rice residue burning. Values represent the number of fires within each 0.05° × 0.05° grid point. For better appreciation of results, color bars have a different range of values. (For interpretation of the references to color in this figure legend, the reader is referred to the Web version of this article.)

large part is burned (Ravindra et al., 2019). The average interannual total regional $PM_{2.5}$ emissions are 245 Gg (standard deviation = 33 Gg) and 406 Gg (standard deviation = 109 Gg) for wheat and rice residue burning, respectively. Fig. 4 also shows that particulate matter emissions in Punjab and Haryana are more homogeneously distributed in the case of wheat stubble, being rice residues emissions more concentrated in the south of Punjab and north of Haryana. This was also noticed using MODIS and VIIRS data by Beig et al. (2020) and Singh et al. (2020) during the cold season.

Fig. 5 presents the interannual variations in total number of fires and regional $PM_{2.5}$ emissions. Fig. 5a shows that the regional total decreased between 2012 and 2015 in the case of wheat, and then increased until 2019. For rice, the number of fires shows relatively constant values between 2012 and 2015, then a significant increase in 2016, and then decline until 2019. These interannual fluctuations in number of fires and consequently in the burned area can have a direct impact on pollutant emissions (e.g. Song et al., 2009), as discussed below. On average (2012–2020), net total emissions from wheat and rice residues were 361 Gg, equivalent to 44% of the total multi-crop emissions of 2016–2017 quantified by Ravindra et al. (2019). Fig. 5c and d also show the regionally-aggregated average daily $PM_{2.5}$ emissions. In this case, as seen in both curves, daily values show a gradual increase from near zero, to then reach a peak around the first and second week of the May and November, respectively for wheat and rice. It is also observed that the daily emissions from rice residues double those generated by the burning of wheat stubble. The shape of the temporal evolution of

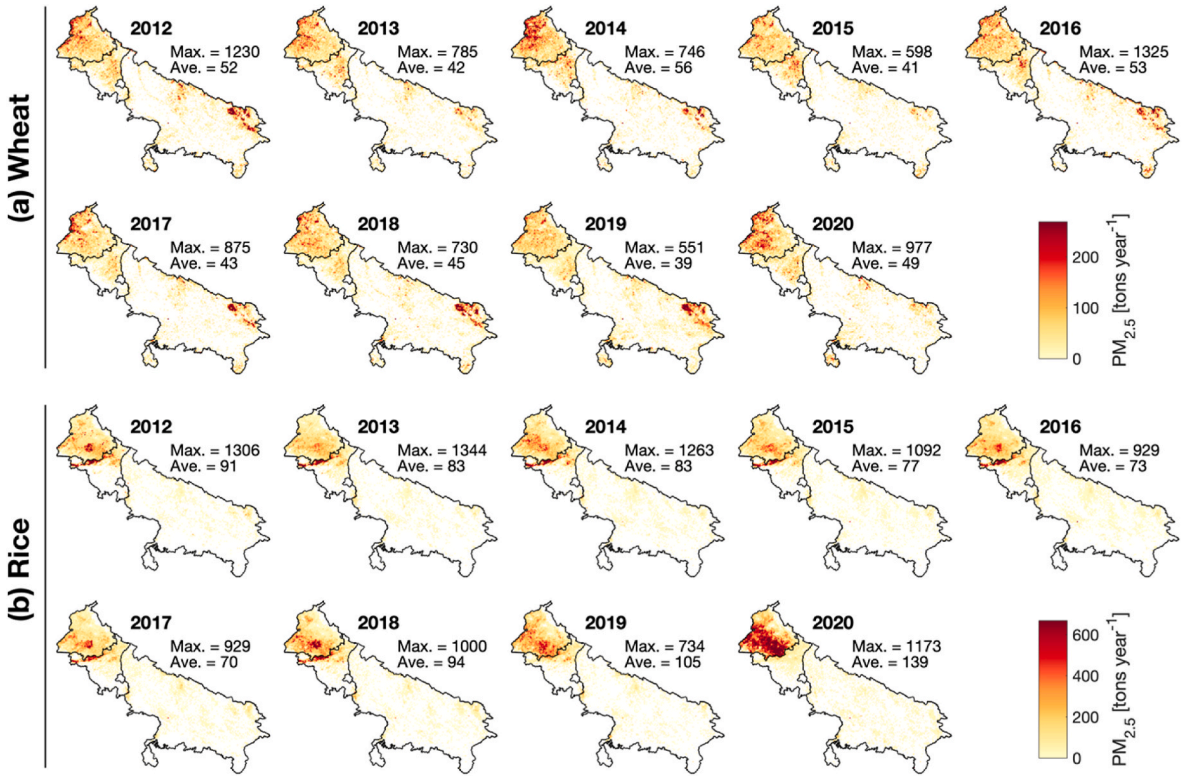

Fig. 4. Maps of $PM_{2.5}$ emissions (per grid; 2012–2020) associated with wheat and rice residue burning. For better appreciation of results, color bars have a different range of values. (For interpretation of the references to color in this figure legend, the reader is referred to the Web version of this article.)

emissions agrees with previously observed number of fires (Fig. 2a).

3.2. Regional MERRA-2 and in-situ surface $PM_{2.5}$ concentration

The interannual mean total surface $PM_{2.5}$ for both wheat and rice periods are displayed in Fig. 6a and b, respectively. $PM_{2.5}$ exhibits both a different magnitude and distribution across the IGP, where emissions associated with rice biomass burning practically doubles the concentrations during wheat residue burning. Also, the spatial distribution of $PM_{2.5}$ during the wheat harvest period tends to concentrate over the eastern part of the IGP, with concentrations higher than $\geq$40 μg m^{-3}. This feature was highlighted by Di Girolamo et al. (2004), who described this accumulation of aerosols over the east IGP as a result of the interaction between topographical and meteorological factors. Conversely, higher $PM_{2.5}$ concentrations are observed along the NW-SE axis of the IGP during the rice harvest period (Fig. 6b), when $PM_{2.5}$ can reach up to $\geq$100 μg m^{-3}. A similar pattern and magnitudes were previously described by Navinya et al. (2020) using MERRA-2 aerosols data (2015–2018), who stated that the pre- and post-monsoon seasons are those with the lowest and highest $PM_{2.5}$ concentrations. Also, similar results were obtained for different periods by Ojha et al. (2020) using the Weather Research and Forecasting model coupled with Chemistry (WRF-Chem) in winter, and by Schnell et al. (2018) using the Geophysical Fluid Dynamics Laboratory Atmospheric Model version 4 (GFDL AM4).

Daily time series of seasonal cycles of MERRA-2 surface $PM_{2.5}$ for wheat and rice residue burning periods are displayed in Fig. 6c and d, respectively. During the 2-month pre-monsoon season (Fig. 6c), surface $PM_{2.5}$ over the IGP averages a concentration of 54 μg m^{-3}, and shows a slight increase from 40 μg m^{-3} to 58 μg m^{-3}, which is indicative of a relatively low temporal variability. Conversely, Fig. 6d shows a sharper rise of surface $PM_{2.5}$ concentrations, from a minimum of 43 μg m^{-3} to a maximum of 138 μg m^{-3} in November, and also a higher regional variability represented by the standard deviation. It is important to note that the shape of the curve in Fig. 6c differs for the case of emissions presented in Fig. 5c, despite being coincident with the seasonality in VIIRS fire count of Fig. 2. Both seasons present contrasting conditions in terms of meteorological factors associated with a higher or lower ventilation and consequently in the capacity of the atmosphere to disperse pollutants. In general, the decline in temperatures and incoming radiative fluxes in winter are responsible for the development of shallow atmospheric boundary layers, which prevents the dispersion of aerosols. The above is enhanced by the lower pressure gradients and consequently winds, and the seasonal suppression of precipitation, conditions that are widespread across the IGP in winter. In this sense, Ojha et al. (2020) found that slightly higher temperatures over eastern IGP allow a deeper boundary layer and a relatively higher ventilation. Similar, a composite analysis by Schnell et al. (2018) revealed that the regional most polluted days in northern India are associated with a lower boundary layer height, high relative humidity, and strong temperature inversions. Moreover, although $PM_{2.5}$ concentration values during wheat harvest is considerably lower than for rice, the average values observed in Fig. 6 are above standard threshold of 25 μg m^{-3} recommended by the World Health Organization.

As pointed out in section 2.2.5, ground data were used to characterize biases in MERRA-2 $PM_{2.5}$ surface concentrations. A comparison between MERRA-2 and ground-truth $PM_{2.5}$ surface concentrations was performed for selected locations, which are displayed in Fig. 1. The combined scatter plot between surface $PM_{2.5}$ concentration and MERRA-2 for available days during wheat and rice residue burning periods is displayed in Fig. S2, and Table 2 shows a more detailed statistical comparison for stations. The linear fit (Fig. S2) indicates a systematic underestimation of surface concentrations by MERRA-2 present in the two periods of the year being compared, with a bias of −45.7 μg m^{-3}. Similar results were obtained using the Modern-Era Retrospective Analysis for Research and Applications Aerosol Reanalysis (MERRAero) product for different locations in Europe by Provençal et al. (2017), in China by Song et al. (2018) and Ma et al. (2020), and also over India by

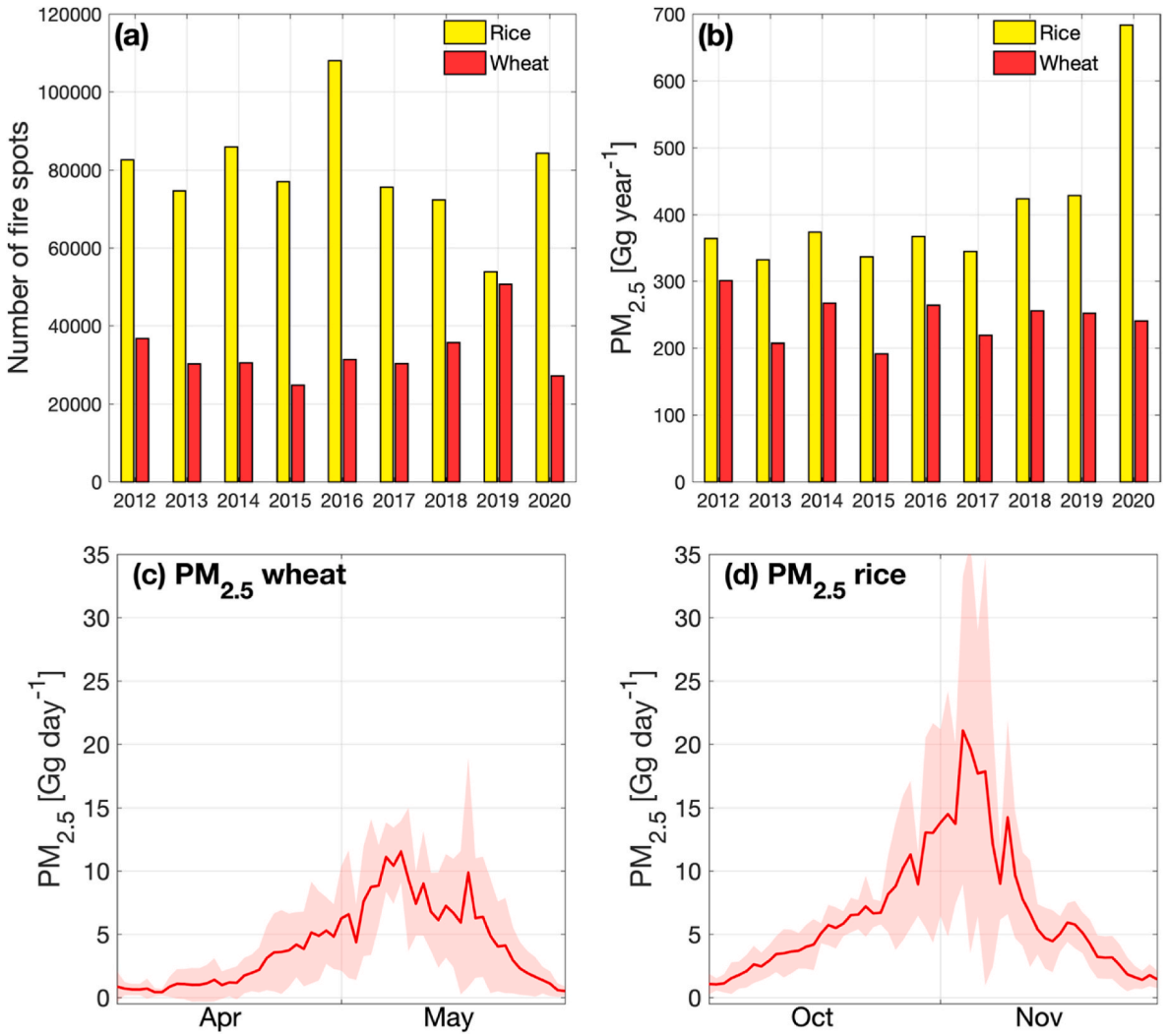

Fig. 5. (a) Total annual (2012–2020) number of fire spots and (b) PM2.5 emissions for rice and wheat residue burning. (c) and (d) are the time series of mean daily regionally-aggregated emissions of $PM_{2.5}$ (solid line) from wheat and rice residue burning, respectively. Shaded area in (c) and (d) denotes the interannual standard deviation.

Mahesh et al. (2019). Nevertheless, a statistically significant R^2 was found ($p = 0$; data now shown), which suggests the possibility of applying a bias correction method, for which a larger ground data set would be necessary. This underestimation may be due to the higher thickness of the atmospheric surface layer represented by MERRA-2, which corresponds to the lowest layer of the GEOS-5 model (Bosilovich et al., 2016). The later considering that ground measurements are typically performed in the first few meters above the land surface, very close to the emission sources.

3.3. Seasonal features of $PM_{2.5}$ emissions and concentration

3.3.1. $p.m._{2.5}$ and fire seasonal metrics

A composite analysis $PM_{2.5}$ concentration anomalies and total emissions was carried out in order to elucidate the relationship with three metrics describing the fire season: total number of fires, seasonally-integrated FRP, and date of peak $PM_{2.5}$ surface concentration. The total number of fires and FRP were integrated for the period between the first and last fire of the corresponding season. The peak $PM_{2.5}$ concentration date was obtained after applying a 5-day moving average filter to each $PM_{2.5}$ time series between the first fire and the last day of the season (May 31st and November 30th, respectively for wheat and rice) as the number of days between the first fire and the maximum value found (peak). Finally, seasonal anomalies were calculated by subtracting the corresponding 9-year interannual average to each year/season time series and grid cell.

Fig. 7 shows the scatter plot between anomalies of MERRA-2 $PM_{2.5}$ concentration and emissions (gridded VIIRS), along with the anomalies of the three above-mentioned fire season metrics for wheat (upper panel) and rice (lower panel). The strong linear relationship between $PM_{2.5}$ concentration and emissions is observed, with significant correlations in both cases: $R^2 = 0.84$ and 0.65 for wheat and rice, respectively. However, a greater dispersion in the case of rice, indicating the likely influence of other factors associated with $PM_{2.5}$ concentrations. Moreover, the strong relationship between biomass generated and emissions suggests that wheat and rice production could potentially be a good statistical predictor of seasonal $PM_{2.5}$ concentration anomalies.

The association between positive anomalies of both $PM_{2.5}$ concentration, emissions and number of fires is stronger for the case of wheat (Fig. 7a and d). On the other hand, positive anomalies in FRP are associated with positive anomalies in $PM_{2.5}$ concentrations and emissions (Fig. 7b), which is less clear in the case of rice (Fig. 7e). The latter suggests that, in the case of wheat, the lower moisture content per unit of biomass burned could determine a higher energy released (FRP), for which FRP could become a discriminating variable (Li et al., 2018). In this way, Fig. 7e shows that FRP does not discriminate positive of

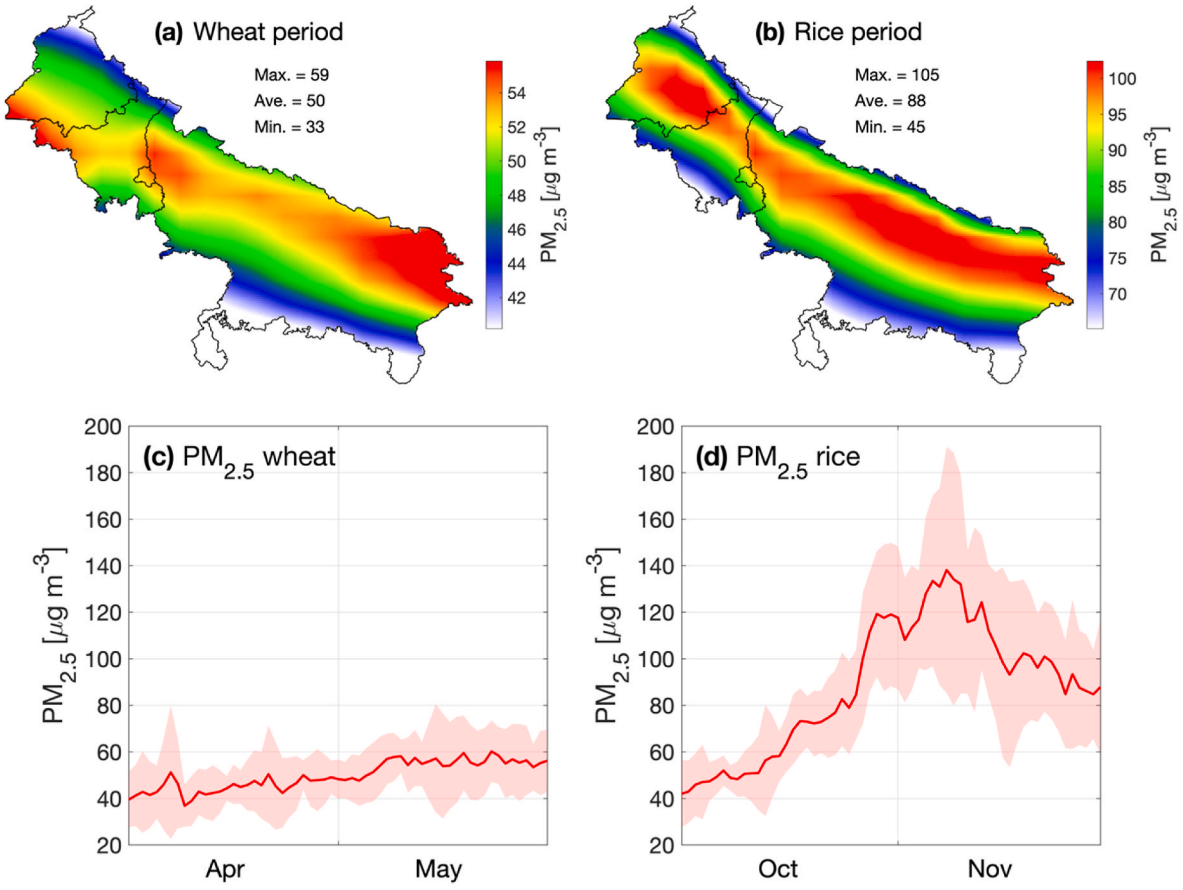

Fig. 6. (a)–(b) Interannual average (2012–2020) of MERRA-2 $PM_{2.5}$ concentration for wheat and rice residue burning periods. (c)–(d) Time series of multi-year (2012–2020) regional average MERRA-2 surface concentration of $PM_{2.5}$ (solid line). For better appreciation of $PM_{2.5}$ distribution, color bars in (a) and (b) have a different range of values. Shaded area in (c) and (d) is the spatial standard deviation.

Table 2
Error statistics Root Mean Square Error (RMSE) and Bias calculated between ground $PM_{2.5}$ stations and MERRA-2.

Station name	Longitude (°)	Latitude (°)	Comparison period	RMSE wheat (μg m^{-3})	RMSE rice (μg m^{-3})	Bias wheat (μg m^{-3})	Bias rice (μg m^{-3})
Kanpur	80.323	26.470	Apr–May 2019 Oct–Nov 2019	58.5	79.4	51.0	41.8
Karnal	77.003	29.695	Apr–May 2019 Oct–Nov 2019	55.6	90.8	50.0	55.6
Mazaffarnagar	77.719	29.472	Apr–May 2019 Oct–Nov 2018	57.1	102.6	46.6	82.8
Patiala	76.367	30.349	Apr–May 2019 Oct–Nov 2019	20.3	45.1	2.9	5.5
New Delhi	77.201	28.636	Apr–May 2019 Oct–Nov 2019	48.2	124.1	38.2	82.5

negative seasonal anomalies in $PM_{2.5}$ concentrations as observed in Fig. 7b. A similar pattern is observed in the case of the number of days to peak $PM_{2.5}$ concentration. Fig. 7c shows that $PM_{2.5}$ positive anomalies during wheat harvest are generally associated with the peak concentration date. Similarly, Fig. 7f shows that later peak dates of $PM_{2.5}$ during the rice harvest period are associated with the higher emissions and concentrations. Additionally, as reported by Ojha et al. (2020), the peak in emissions from crop residue burning could represent the beginning of the decrease in the relative contribution of biomass burning to total air pollution.

3.3.2. *Meteorological drivers of $PM_{2.5}$ concentrations*

Air pollution involves emissions and factors influencing accumulation, dispersion, or chemical reactions of pollutants (Grivas et al., 2008). A composite analysis of $PM_{2.5}$ concentration anomalies and total emissions along with meteorological drivers was performed in order to explore the association between seasonal anomalies in planetary boundary layer height (PBLH), wind speed and inversion strength, for the period between the first and last detected fires. Fig. 8 shows the scatter plot between $PM_{2.5}$ concentration and emissions, and the anomalies of the three selected meteorological variables. Fig. 8a shows that both positive and negative anomalies in PBLH are observed during days of high emission and $PM_{2.5}$ concentration. However, negative anomalies in PBLH are dominant in days of high emission and $PM_{2.5}$ concentration of rice residue burning (Fig. 8d). The latter indicates that the relationship between PBLH and concentration of pollutants is less evident on a seasonal scale. Thus, in the case of burning of wheat residues (Fig. 8a), PBLH anomalies slightly discriminate between positive or negative $PM_{2.5}$ concentrations. However, Fig. 8d shows a higher number of points in the quadrant of positive $PM_{2.5}$ anomalies. On the other hand,

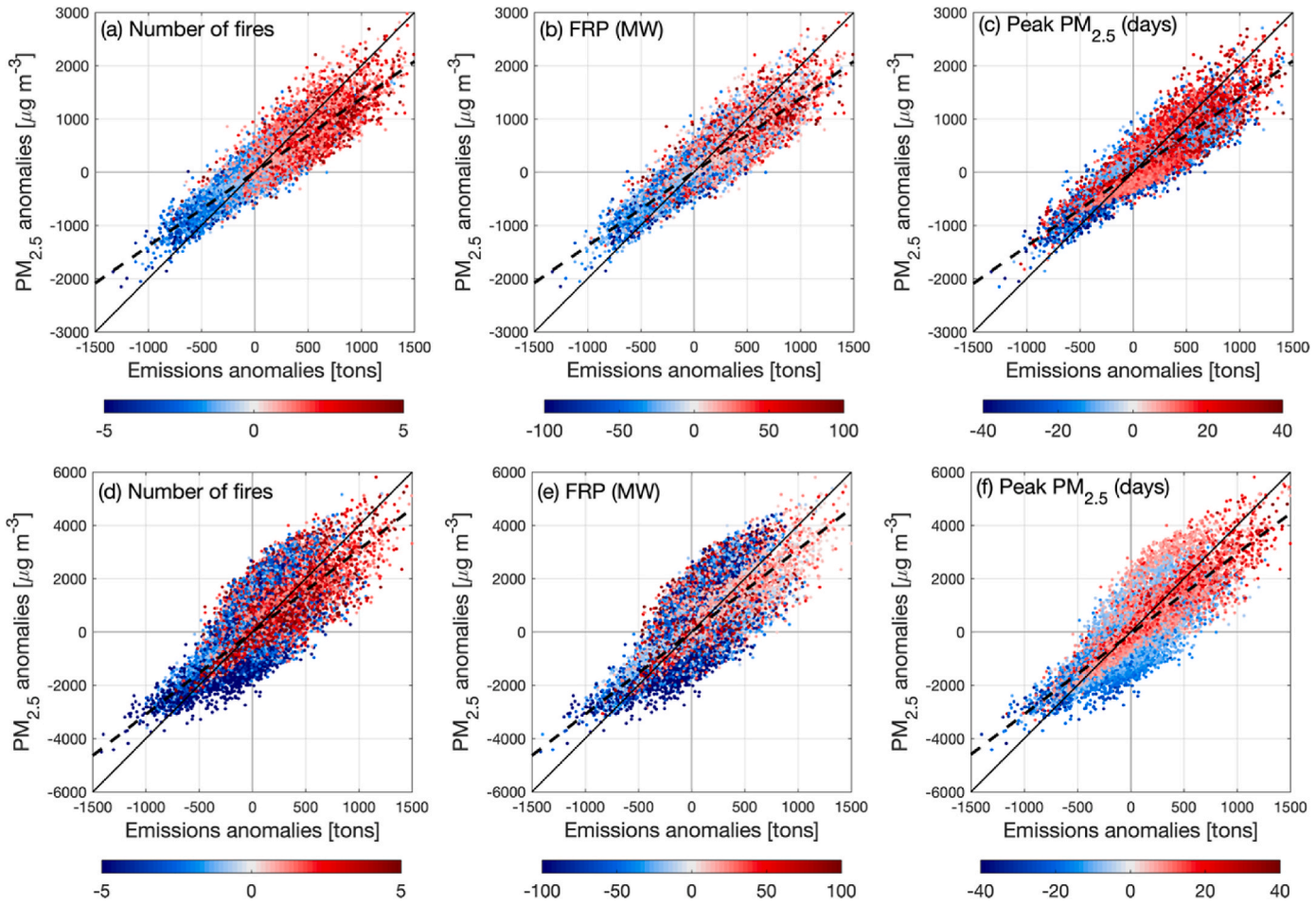

Fig. 7. Scatter plot between seasonally-integrated total $PM_{2.5}$ emissions, surface $PM_{2.5}$ concentration, and (a) number of fires, (b) seasonally-integrated FRP (color scale in MW), and (c) peak $PM_{2.5}$ concentration date as numbers of days between first detected fire and maximum $PM_{2.5}$ concentration (color scale in days), for (a)–(c) wheat and (d)–(f) rice. For better appreciation, *y*-axis of the upper and lower panels has a different range of values, and values between the 33rd and 66th percentiles of the corresponding variables shown in color scale were removed. (For interpretation of the references to color in this figure legend, the reader is referred to the Web version of this article.)

wind speed anomalies (Fig. 8b and e) show a higher discrimination between positive or negative anomalies of $PM_{2.5}$. In this sense, seasonal anomalies in surface (10-m) wind speed seem to capture the effect on horizontal ventilation (Liu et al., 2018b). Schnell et al. (2018) described a similar statistical relationship between $PM_{2.5}$ concentration and wind speed on a daily scale over the IGP. In addition, the dominant surface NW-SE flow over the IGP might explain this weak seasonal relationship, since, for example, higher local ventilation conditions in Punjab could enhance the transport of pollutants to Uttar Pradesh, making the above-described relationships less consistent at the regional level. Further research would be necessary to validate this hypothesis.

The relationship between $PM_{2.5}$ concentrations, emissions and the inversion strength (Fig. 8c and f) suggests a stronger seasonal influence of this meteorological variable. The observed inversion strength is in the range of values obtained by Schnell et al. (2018) using a dynamical meteorological model during high surface $PM_{2.5}$ concentration days. In the case of the wheat residues burning, for a specific amount of burned residues (emissions), $PM_{2.5}$ concentrations will be influenced by the anomalies in the inversion strength. This relationship appears much clearer for the case of wheat, where stronger thermal inversion layers, which means more potential accumulation of particles, will strongly determine $PM_{2.5}$ concentrations for a given amount of residue burned in the field.

The relationship between meteorological variables and $PM_{2.5}$ concentrations was summarized by the PCA applied to regional averages of $PM_{2.5}$ concentrations and meteorological variables. Results are presented in Fig. 9 for wheat and rice, and for the first two principal components, which explain an 84.7% and 61.5% of the total variance, respectively for wheat and rice. Fig. 9 shows some differences in the relationship between $PM_{2.5}$ and environmental variables for wheat and rice residue burning. In the case of wheat (Fig. 9a), PC 2 generally separates $PM_{2.5}$ from wind speed and the inversion strength, while the relationship between $PM_{2.5}$ and the remaining variables is almost orthogonal, indicating a weak correlation (angle between vectors near 90°). An interesting feature corresponds to the positive relationship between $PM_{2.5}$ and air temperature during the wheat harvest period (pre-monsoon), which suggests that higher concentrations of $PM_{2.5}$ during warm/dry conditions might be associated with, for example, a late monsoon onset. The latter is also suggested by the negative relationship between $PM_{2.5}$ and wind speed and the inversion strength in PC 1, since stronger winds and a weakened inversion layer are associated with stronger convection and development of the mixing layer, which is in turn associated with higher sensible heat fluxes (Mues et al., 2017). However, further research is needed to validate this hypothesis. Fig. 9a also shows PC 1 the positive relationship between $PM_{2.5}$ and meteorological variables PBLH, air temperature (T2M) and surface layer height (SLH). Conversely, $PM_{2.5}$ is negatively correlated with relative humidity (RH). The latter can be also associated with the higher PM2.5 concentrations during drier pre-monsoon conditions. On the other hand, Fig. 9b shows that PC 1 clearly separates the relationship between SLH, T2M

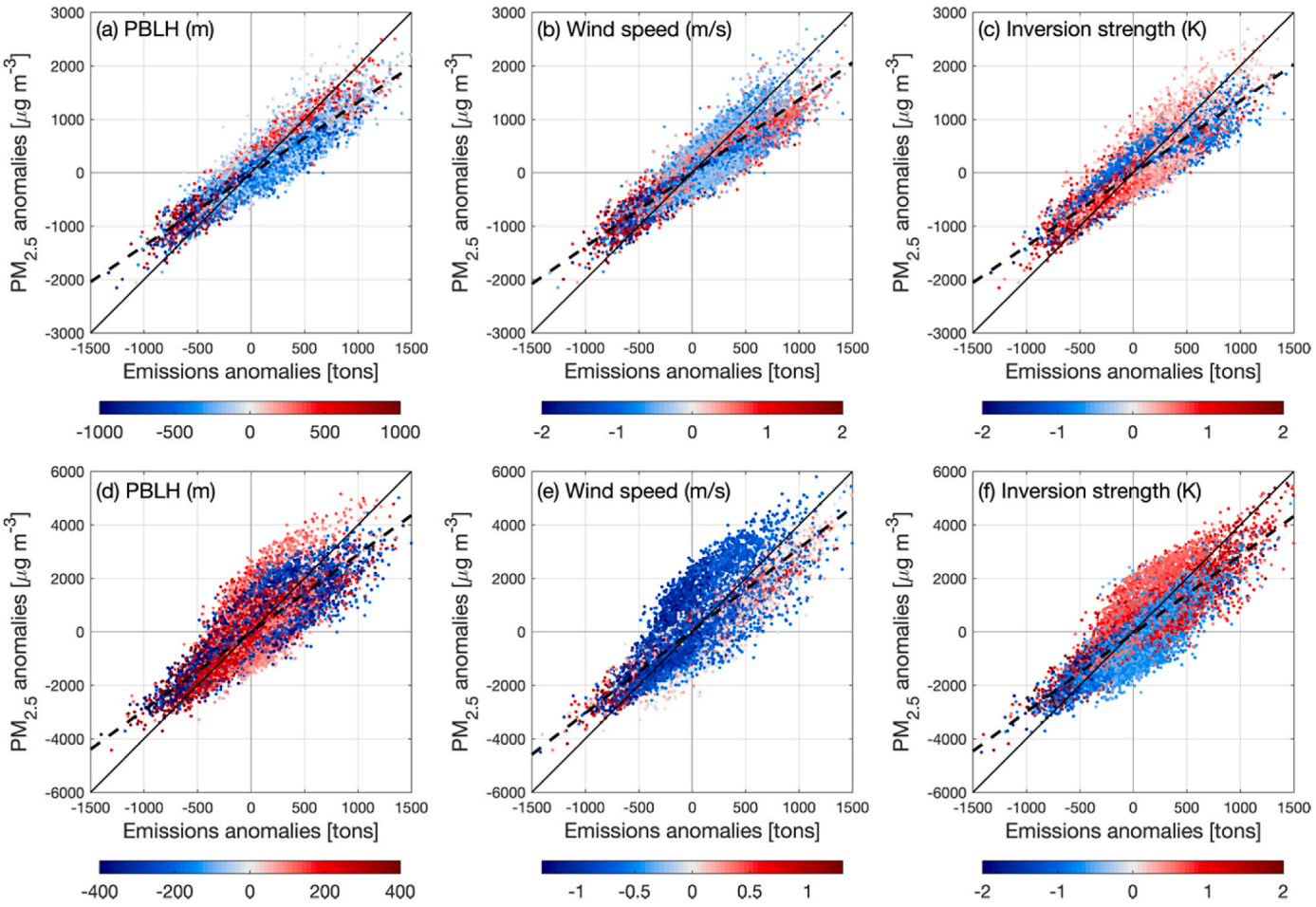

Fig. 8. Scatter plot between seasonally-integrated total $PM_{2.5}$ emissions, surface $PM_{2.5}$ concentration, and (a) average PBLH (color scale in m), (b) average wind speed (color scale in m s^{-1}), and (c) average inversion strength (color scale in K), for (a)–(c) wheat and (d)–(f) rice. For better appreciation, *y*-axis of the upper and lower panels has a different range of values, and values between the 33rd and 66th percentiles of the corresponding variables shown in color scale were removed. (For interpretation of the references to color in this figure legend, the reader is referred to the Web version of this article.)

and PBLH from wind speed, but not from $PM_{2.5}$. However, a positive relationship is observed between $PM_{2.5}$ and the inversion strength in PC 2, while a negative relationship is observed between $PM_{2.5}$ and wind speed. In this case, $PM_{2.5}$ concentrations during the post-monsoon season show a greater association with inversion strength and air humidity, which may be the result of the influence of large-scale synoptic meteorological factors controlling the properties of the atmospheric boundary layer (Gutiérrez et al., 2013; Schnell et al. 2018) rather than the variables associated with surface conditions (2-m air temperature, surface layer height, PBLH). The latter could be explained by the lower variability in temperatures during the cold and dry season, so that, unlike the wheat harvest period, the meteorological factors associated with the dispersion of pollutants would be able to better discriminate $PM_{2.5}$ concentrations.

3.4. Uncertainties and limitations

Despite not being the primary objective of this work, it is worthwhile to compare the obtained regional emissions from crop residue burning with other published works for the IGP where similar approaches based on active fire products and crop production census data were used along with the associated uncertainties. Singh et al. (2020) estimated 137 Gg and 57 Gg of PM2.5 emissions in Punjab and Haryana in 2017–2018 from crop residue burning, authors that considered more crops in the annual biomass production but a shorter time period (2018). Similar, a total of 141 Gg/year were estimated by Beig et al. (2020) in Punjab and Haryana by *kharif* (monsoon) season crops burning in 2018. Although these values are within the range of results presented in this work, differences in estimations of particulate matter emissions are explained by all the steps necessary for their calculation, including the input data (crop production) and the parameters for the conversion from production to biomass burned in the field. In this way, a sensitivity analysis would be necessary to investigate the relative effect of each parameter on the estimations. Furthermore, an important parameter corresponds to the emission factor (*EF*), which has been determined using multiple approaches, including laboratory analysis, whose value is highly variable in the literature. In this work we used parameters that allow the results to be comparable with previous studies over the same region.

Another source of differences between results presented in this work and the literature corresponds to the satellite sensor. VIIRS and MODIS are among the most used sensors; however, their ability to detect fires is highly variable. The comparison of VIIRS and MODIS by Vadrevu and Lasko (2018) showed a higher number of fires detected by VIIRS in a factor of 4.8 in relation to MODIS Aqua and Terra in Punjab. These differences influence the temporal and spatial allocation of crop biomass burned to single fires, affecting seasonal patterns and balances. Moreover, although VIIRS has a greater ability to detect fires than MODIS, its temporal coverage may not be high enough to capture short duration fires. Local experience indicates that crop residue burning takes place typically in the late afternoon, lasting for a few hours, which makes difficult the detection of small fires. Likewise, cloud cover can significantly prevent the detection of small/short duration fires, as reported by

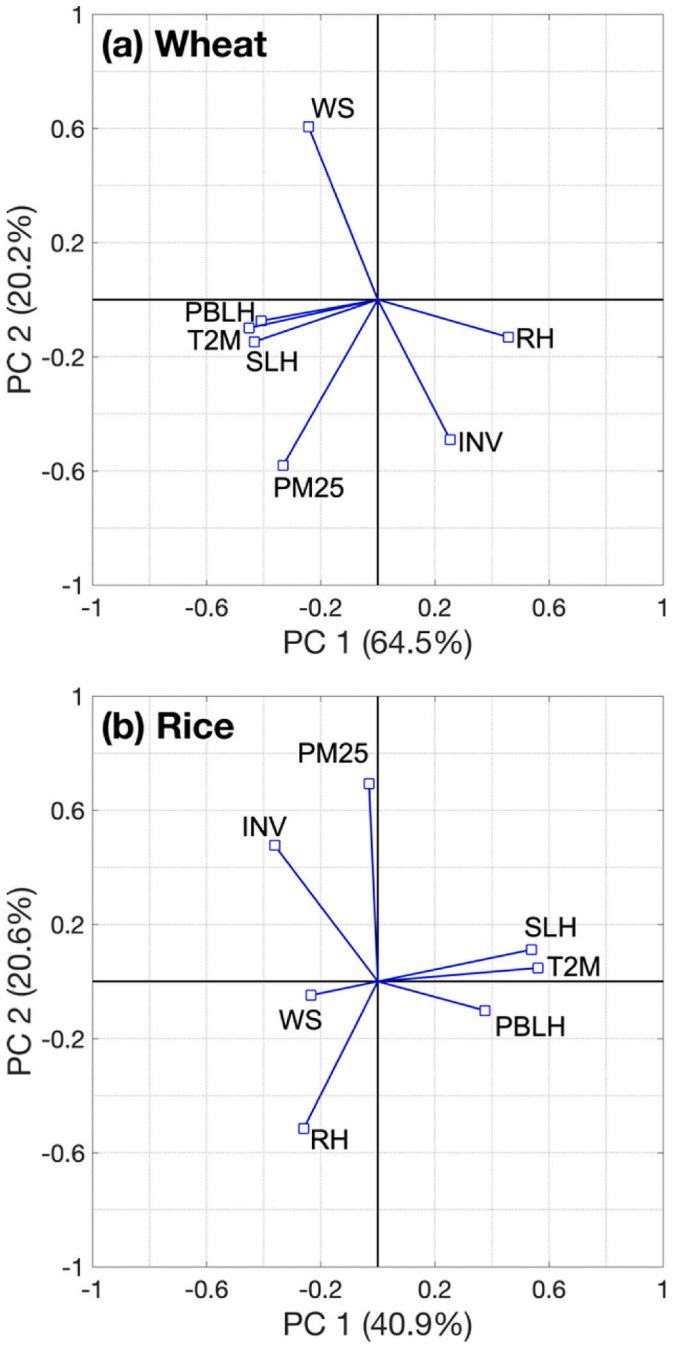

Fig. 9. Biplot displaying the two first principal components (PC 1 and PC 2) and their corresponding explained variance (in %) derived from a PCA applied to daily regional mean of $PM_{2.5}$ concentrations (PM25), wind speed (WS), the inversion strength (INV), planetary boundary layer height (PBLH), surface layer height (SLH), 2-m air temperature (T2M), and 2-m relative humidity (RH). Vectors denote the contribution of a single variable to the PC.

Schroeder and Csiszar, 2014. In a similar way, according to Liu et al. (2019), small and scattered fires are also underestimated by MODIS. Notwithstanding, and considering all these sources of uncertainty and errors, the seasonal patterns and associated anomalies should be well captured by the approach adopted in this work.

Finally, we assumed that during April–May and October–November the detected fires were associated with wheat and rice residue burning, respectively, but other crops can be also present over the region, whose residues are prone to being burned (Singh et al., 2020). However, since wheat and rice are the dominant crops in terms of cultivated area, the calculated $PM_{2.5}$ emissions should represent the variability in the burning of residues of these two dominant crops.

4. Conclusions

In this study we present a multi-year analysis of $PM_{2.5}$ emissions associated with the burning of wheat and rice residues in terms of their spatial and temporal patterns. We focused on pre- and post-monsoon fire episodes across the IGP to generate a high-resolution and multi-annual product of emissions using the full VIIRS time span (2012–2020), emphasizing the seasonal patterns of $PM_{2.5}$ emissions, concentrations, and associated factors. $PM_{2.5}$ emissions were estimated by using both crop production and VIIRS satellite active fire products. Obtained results in terms of emissions are within the range of values from previous inventories reported for the same region using similar approaches.

Results allow a better understanding of the seasonal variability in pollutant emissions and consequences in terms of air pollution for a vast region of India. While a high concentration of fires is observed in Punjab and Haryana, fires in Uttar Pradesh can contribute to total emissions during wheat harvest. Results shows that both the number of fires and $PM_{2.5}$ emissions from during rice harvest roughly double those from wheat residue burning. The observed relationships between $PM_{2.5}$ concentrations and emissions with fire season metrics offer opportunities for monitoring crop residue burning activities and their effect on regional air pollution. The latter includes information and actionable products regarding potential air pollution anomalies, especially for extreme episodes, in part thanks to the possibility of accessing high resolution satellite data.

The use of MERRA-2 reanalysis-based seasonal meteorological anomalies to assess the relationships with $PM_{2.5}$ concentrations and emissions shows that the relationships between air pollution and meteorological factors affecting its distribution in the air column are clearer for the rice harvest period. Factors associated, for example, with the amount of biomass produced and burned in the field has a higher relationship with emissions during the wheat harvest. The latter opens the possibility of using monthly-scale seasonal climate forecasting along with crop production projections to estimate anomalies in surface air pollution associated with crop residue burning. This could also be done on larger time scales, given the strong relationship between emissions and concentrations. On the other hand, since the highest concentration of pollutants is observed during the rice harvest, reaching a regional peak during the first days of November, a later rice plantation and subsequent harvest date should in turn delay the date of occurrence of this peak, which could have negative consequences given the unfavorable meteorological conditions for the dispersion of pollutants during winter.

In terms of meteorological drivers, both the anomalies and the PCA-based analysis revealed a varying relationship between variables and $PM_{2.5}$ for wheat and rice harvest periods. Both periods show a higher association with variables that characterize the atmospheric boundary layer, rather than surface conditions; however, this association may be due to different reasons. In the case of the wheat harvest period, the delay in the onset of the rainy season or the occurrence of prolonged dry spells can favor the accumulation of pollutants in the atmosphere. On the other hand, during the rice harvest in winter, the large-scale synoptic variability factors controlling the daily and seasonal development of the atmospheric boundary layer could be more relevant. In both cases, the results suggest that statistical and physically-based models could be potentially used to improve the seasonal forecast of $PM_{2.5}$ concentrations from variables such as rainfall and pressure gradients (e.g. geopotential height) along with crop production projections (Leung et al., 2018; Baklanov and Zhang, 2020).

CRediT authorship contribution statement

Carlo Montes: Conceptualization, Data curation, Formal analysis,

Investigation, Methodology, Resources, Software, Validation, Visualization, Writing – original draft, Writing – review & editing. **Tek Sapkota:** Funding acquisition, Project administration, Writing – review & editing. **Balwinder Singh:** Writing – review & editing.

Declaration of competing interest

The authors declare that they have no known competing financial interests or personal relationships that could have appeared to influence the work reported in this paper.

Acknowledgements

This work was carried out by International Maize and Wheat Improvement Center (CIMMYT) with support of the CGIAR research program on Climate Change, Agriculture and Food Security (CCAFS). CCAFS′ work is supported by CGIAR Fund Donors and through bilateral funding agreements. For details please visit https://ccafs.cgiar.org/donors. The views expressed in this paper cannot be taken to reflect the official opinions of these organizations.

Appendix A. Supplementary data

Supplementary data to this article can be found online at https://doi.org/10.1016/j.aeaoa.2022.100154.

References

Allen, R.G., Pereira, L.S., Raes, D., Smith, M., 1998. Crop Evapotranspiration. Guidelines for Computing Crop Water Requirements, 300. In: FAO Irrigation and Drainage Paper 56. FAO, Rome, 487 6541.

Andreae, M.O., 2019. Emission of trace gases and aerosols from biomass burning - an updated assessment. Atmos. Chem. Phys. 19, 8523–8546.

Azhar, R., Zeeshan, M., Fatima, K., 2019. Crop residue open field burning in Pakistan; multi-year high spatial resolution emission inventory for 2000-2014. Atmos. Environ. 208, 20–33.

Baklanov, A., Zhang, Y., 2020. Advances in air quality modeling and forecasting. Global Transitions 2, 261–270.

Balwinder-Singh, McDonald, A.J., Srivastava, A.K., Gerard, B., 2019. Tradeoffs between groundwater conservation and air pollution from agricultural fires in northwest India. Nat. Sustain. 2, 580–583.

Beig, G., Sahu, S.K., Singh, V., Tikle, S., Sobhana, S.B., Gargeva, P., Ramakrishna, K., Rathod, A., Murthy, B.S., 2020. Objective evaluation of stubble emission of North India and quantifying its impact on air quality of Delhi. Sci. Total Environ. 709, 136126.

Bhattacharyya, P., Bisen, J., Bhaduri, D., Priyadarsini, S., Munda, S., Chakraborti, M., Adak, T., Panneerselvam, P., Mukherjee, A.K., Swain, S. Lf, Dash, P.K., Padhy, S.R., Nayak, A.K., Pathak, H., Kumar, S., Nimbrayan, P., 2021. Turn the wheel from waste to wealth: economic and environmental gain of sustainable rice straw management practices over field burning in reference to India. Sci. Total Environ. 775, 145896.

Bosilovich, M.G., Lucchesi, R., Suarez, M., 2016. MERRA-2: File Specification. GMAO Office Note No. 9 (Version 1.1), 73 pp. Available from. http://gmao.gsfc.nasa.gov/pubs/office_notes, 73.

Bray, C.D., Battye, W.H., Aneja, V.P., 2019. The role of biomass burning agricultural emissions in the Indo-Gangetic Plains on the air quality in New Delhi, India. Atmos. Environ. 218, 116983.

Buchard, V., da Silva, A.M., Randles, C.A., Colarco, P., Ferrare, R., Hair, J., Hostetler, C., Tackett, J., Winker, D., 2016. Evaluation of the surface PM2.5 in version 1 of the NASA MERRA aerosol reanalysis over the United States. Atmos. Environ. 125, 100–111.

Chin, M., Ginoux, P., Kinne, S., Torres, O., Holben, B., Duncan, B., Martin, R., Logan, J., Higurashi, A., Nakajima, T., 2002. Tropospheric aerosol optical thickness from the GOCART model and comparisons with satellite and sun photometer measurements. J. Atmos. Sci. 59, 461–483.

Chowdhury, S., Dey, S., Di Girolamo, L., Smith, K.R., Pillarisetti, A., Lyapustin, A., 2019. Tracking ambient PM2.5 build-up in Delhi national capital region during the dry season over 15 years using a high-resolution (1 km) satellite aerosol dataset. Atmos. Environ. 204, 142–150.

Dey, S., Di Girolamo, L., van Donkelaar, A., Tripathi, S.N., Gupta, T., Mohan, M., 2012. Variability of outdoor fine particulate (PM2.5) concentration in the Indian Subcontinent: a remote sensing approach. Remote Sens. Environ. 127, 153–161.

Di Girolamo, L., Bond, T.C., Bramer, D., Diner, D.J., Fettinger, F., Kahn, R.A., Martonchik, J.V., Ramana, M.V., Ramanathan, V., Rasch, P.J., 2004. Analysis of Multi-angle Imaging SpectroRadiometer (MISR) aerosol optical depths over greater India during winter 2001-2004. Geophys. Res. Lett. 31, L23115. https://doi.org/10.1029/2004GL021273.

Friedl, M.A., Sulla-Menashe, D., Tan, B., Schneider, A., Ramankutt, N., Sibley, A., Huang, X., 2010. MODIS Collection 5 global land cover: algorithm refinements and characterization of new datasets. Remote Sens. Environ. 114, 168–182.

Gadde, B., Bonnet, S., Menke, C., Garivait, S., 2009. Air pollutant emissions from rice straw open field burning in India, Thailand and the Philippines. Environ. Pollut. 157, 1554–1558.

Grivas, G., Chaloulakou, A., Kassomenos, P., 2008. An overview of the PM10 pollution problem. Sci. Total Environ. 389. In: The Metropolitan Area of Athens, Greece. Assessment of Controlling Factors and Potential Impact of Long Range Transport, pp. 165–177.

Gupta, S., Agarwal, R., Mittal, S.K., 2016. Respiratory health concerns in children at some strategic locations from high PM levels during crop residue burning episodes. Atmos. Environ. 137, 127–134.

Gutiérrez, J.M., San-Martín, D., Brands, S., Manzanas, R., Herrera, S., 2013. Reassessing statistical downscaling techniques for their robust application under climate change conditions. J. Clim. 26, 171–188.

Hays, M.D., Fine, P.M., Geron, C.D., Kleeman, M.J., Gullett, B.K., 2005. Open burning of agricultural biomass: physical and chemical properties of particle-phase emissions. Atmos. Environ. 39, 6747–6764.

IQAir, 2019. 2019 World Air Quality Report, p. 35p.

Jain, N., Bhatia, A., Pathak, H., 2014. Emission of air pollutants from crop residue burning in India. Aerosol Air Qual. Res. 14, 422–430.

Jethva, H., Chand, D., Torres, O., Gupta, P., Lyapustin, A., Patadia, F., 2018. Agricultural burning and air quality over Northern India: a synergistic analysis using NASA's A-train satellite data and ground measurements. Aerosol Air Qual. Res. 18, 1756–1773.

Jethva, H., Torres, O., Field, R.D., Lyapustin, A., Gautam, R., Kayetha, V., 2019. Connecting crop productivity, residue fires, and air quality over northern India, 2019 Sci. Rep. 9, 16594.

Kaskaoutis, D.G., Kumar, S., Sharma, D., Singh, R.P., Kharol, S.K., Sharma, M., Singh, A. K., Singh, S., Singh, A., Singh, D., 2014. Effects of crop residue burning on aerosol properties, plume characteristics, and long-range transport over northern India. J. Geophys. Res. Atmos. 119 (9), 5424–5444.

Kumar, P., Kumar, S., Joshi, L., 2015. Socioeconomic and Environmental Implications of Agricultural Residue Burning: a Case Study of Punjab. Springer, New Delhi.

Leung, D.M., Tai, A.P.K., Mickley, L.J., Moch, J.M., van Donkelaar, A., Shen, L., V, R., Martin, 2018. Synoptic meteorological modes of variability for fine particulate matter (PM2.5) air quality in major metropolitan regions of China. Atmos. Chem. Phys. 18, 6733–6748.

Li, F., Zhang, X., Kondragunta, S., Roy, D.P., 2018. Investigation of the fire radiative energy biomass combustion coefficient: a comparison of polar and geostationary satellite retrievals over the Conterminous United States. J. Geophys. Res.-Biogeosci. 123, 722–739.

Li, F., Zhang, X., Kondragunta, S., 2020. Biomass burning in Africa: an investigation of fire radiative power missed by MODIS using the 375 m VIIRS active fire product. Rem. Sens. 12 (10), 1561.

Liu, T., Marlier, M.E., DeFries, R.S., Westervelt, D.M., Xia, K.R., Fiore, A.M., Mickley, L. J., Cusworth, D.H., Milly, G., 2018a. Seasonal impact of regional outdoor biomass burning on air pollution in three Indian cities: Delhi, Bengaluru, and Pune. Atmos. Environ. 172, 83–92.

Liu, D., Yan, W., Kang, Z., Liu, A., Zhu, Y., 2018b. Boundary-layer features and regional transport process of an extreme haze pollution event in Nanjing, China. Atmos. Pollut. Res. 9, 1088–1099.

Liu, T., Marlier, M.E., Karambelas, A., Jain, M., Singh, S., Singh, M.K., Gautam, R., DeFries, R.S., 2019. Missing emissions from post-monsoon agricultural fires in northwestern India: regional limitations of MODIS burned area and active fire products. Environ. Res. Commun. 1, 011007.

Liu, T., Mickley, L.J., Singh, S., Jain, M., DeFries, R.S., Marlier, M.E., 2020. Crop residue burning practices across north India inferred from household survey data: bridging gaps in satellite observation. Atmos. Environ. X., 100091

Ma, J., Xu, J., Qu, Y., 2020. Evaluation on the Surface PM2.5 Concentration over China Mainland from NASA's MERRA-2. Atmospheric Environment. https://doi.org/10.1016/j.atmosenv.2020.117666.

Mahesh, B., Rama, B.V., Spandana, B., Sarma, K.N., Niranjan, K., Sreekanth, V., 2019. Evaluation of MERRAero PM2.5 over Indian cities. Adv. Space Res. 64, 328–334.

Mittal, S.K., Singh, N., Agarwal, R., Awasthi, A., Gupta, P.K., 2009. Ambient air quality during wheat and rice crop stubble burning episodes in Patiala. Atmos. Environ. 43, 238–244.

Mues, A., Rupakheti, M., Münkel, C., Lauer, A., Bozem, H., Hoor, P., Butler, T., Lawrence, M.G., 2017. Investigation of the mixing layer height derived from ceilometer measurements in the Kathmandu Valley and implications for local air quality. Atmos. Chem. Phys. 17, 8157–8176.

Nair, M., Bherwani, H., Kumar, S., Gulia, S., Goyal, S., Kumar, R., 2020. Assessment of contribution of agricultural residue burning on air quality of Delhi using remote sensing and modelling tools. Atmos. Environ. 230, 117594.

Navinya, C.D., Vinoj, V., Pandey, S.K., 2020. Evaluation of PM2.5 surface concentrations simulated by NASA's MERRA Version 2 aerosol reanalysis over India and its relation to the air quality index. Aerosol Air Qual. Res. 20, 1329–1339.

Ojha, N., Sharma, A., Kumar, M., Girach, I., Ansari, T.U., Sharma, S.K., Singh, N., Pozzer, A., Gunthe, S.S., 2020. On the widespread enhancement in fine particulate matter across the Indo-Gangetic Plain towards winter. Sci. Rep. 10, 5862.

Pant, P., Shukla, A., Kohl, S.D., Chow, J.C., Watson, J.G., Harrison, R.H., 2015. Characterization of ambient PM2.5 at a pollution hotspot in New Delhi, India and inference of sources. Atmos. Environ. 109, 178–189.

Provençal, S., Buchard, V., da Silva, A.M., Leduc, R., Barrette, N., 2017. Evaluation of PM surface concentrations simulated by version 1 of NASA's MERRA aerosol reanalysis over Europe. Atmos. Pollut. Res. 8, 374–382.

Ravindra, K., Singh, T., Mor, S., 2019. Emissions of air pollutants from primary crop residue burning in India and their mitigation strategies for cleaner emissions. J. Clean. Prod. 208, 261–273.
Rienecker, M., Suarez, M., Gelaro, R., Todling, R., Bacmeister, J., Liu, E., Bosilovich, M., Schubert, S., Takacs, L., Kim, G.K., Bloom, S., Chen, J., Collins, D., Conaty, A., Da Silva, A., Gu, W., Joiner, J., Koster, R., Lucchesi, R., Woollen, J., 2011. MERRA: NASA's Modern-Era retrospective analysis for research and applications. J. Clim. 24, 3624–3648.
Roberts, G., Wooster, M.J., Lagoudakis, E., 2009. Annual and diurnal african biomass burning temporal dynamics. Biogeosciences 6, 849–866.
Sahai, S., Sharma, C., Singh, D.P., Dixit, C.K., Singh, N., Sharma, P., Singh, K., Bhatt, S., Ghude, S., Gupta, V., Gupta, R.K., Tiwari, M.M., Garg, S.C., Mitra, A.P., Gupta, P.K., 2007. A study for development of emission factors for trace gases and carbonaceous particulate species from in situ burning of wheat straw in agricultural fields in India. Atmos. Environ. 41, 9173–9186.
Sahu, L.K., Sheel, V., Pandey, K., Yadav, R., Saxena, P., Gunthe, S., 2015. Regional biomass burning trends in India: analysis of satellite fire data. J. Earth Syst. Sci. 124, 1377–1387.
Sahu, S.K., Mangaraj, P., Beig, G., Samal, A., Pradhan, C., Dash, S., Tyagi, B., 2021. Quantifying the high resolution seasonal emission of air pollutants from crop residue burning in India. Environ. Pollut. 286, 117165.
Sarkar, C., Kumar, V., Sinha, V., 2013. Massive emissions of carcinogenic benzenoids from paddy residue burning in north India. Curr. Sci. 104, 1703–1709.
Schnell, J.L., Naik, V., Horowitz, L.W., Paulot, F., Mao, J., Ginoux, P., Zhao, M., Ram, K., 2018. Exploring the relationship between surface PM2:5 and meteorology in Northern India. Atmos. Chem. Phys. 18, 10157–10175.
Schroeder, W., Oliva, P., Giglio, L., Csiszar, I.A., 2014. The New VIIRS 375 m active fire detection data product: algorithm description and initial assessment. Remote Sens. Environ. 143, 85–96.
Sekar, I., Pal, S., 2012. Rice and wheat crop productivity in the Indo-Gangetic Plains of India: changing pattern of growth and future strategies. Indian J. Agric. Econ. 67, 238–252.
Sembhi, H. M. Wooster, Zhang, T., Sharma, S., Singh, N., Agarwal, S., Boesch, H., Gupta, S., Misra, A., Tripathi, S.N., Mor, S., Khaiwal, R., 2020. Post-monsoon air quality degradation across Northern India: Assessing the impact of policy-related shifts in timing and amount of crop residue burnt. Environ. Res. Lett. https://doi.org/10.1088/1748-9326/aba714.
Singh, T., Biswal, A., Mor, S., Ravindra, K., Singh, V., Mor, S., 2020. A high-resolution emission inventory of air pollutants from primary crop residue burning over Northern India based on VIIRS thermal anomalies. Environ. Pollut. 266, 115132.
Song, Y., Liu, B., Miao, W., Chang, D., Zhang, Y., 2009. Spatiotemporal variation in nonagricultural open fire emissions in China from 2000 to 2007. Glob. Bio-geochem. Cy. 23, GB2008. https://doi.org/10.1029/2008GB003344.
Song, Z., Fua, D., Zhang, X., Wu, Y., Xia, X., He, J., Han, X., Zhang, R., Che, H., 2018. Diurnal and seasonal variability of PM2.5 and AOD in North China plain: comparison of MERRA-2 products and ground measurements. Atmos. Environ. 191, 70–78.
Streets, D.G., Woo, K.F.J.-H., Carmichael, G.R., 2005. Biomass burning in Asia: annual and seasonal estimates and atmospheric emissions. Global Biogeochem. Cycles 17. https://doi.org/10.1029/2003GB002040.
Vadrevu, K., Lasko, K., 2018. Intercomparison of MODIS AQUA and VIIRS I-Band fires and emissions in an agricultural landscape - implications for air pollution research. Rem. Sens. 10, 978. https://doi.org/10.3390/rs10070978.
Zhang, X., Lua, Y., Wang, Q., Qian, X., 2019. A high-resolution inventory of air pollutant emissions from crop residue burning in China. Atmos. Environ. 213, 207–214.